Optimization of Transmission Parameters in Fast Pulse-Echo Ultrasound Imaging using Sparse Recovery

Ozan Çakıroğlu †*, Eduardo Pérez *, Florian Roemer †, Martin Schiffner‡
Fraunhofer Institute for Nondestructive Testing IZFP, Saarbrucken, Germany,†
Technische Universität Ilmenau, Ilmenau, Germany,*
Ruhr-Universität Bochum, Bochum, Germany ‡,

***Abstract*—In pulse-echo ultrasound imaging, the goal is to achieve a certain image quality while minimizing the duration of the signal acquisition. In the past, fast ultrasound imaging methods applying sparse signal recovery have been implemented by accepting a single pulse-echo measurement. However, they have experienced a certain amount of reconstruction error. In sparse signal recovery, reducing the correlation between the samples of the measurements observed by the different receivers is beneficial for lowering the reconstruction error. Exploiting the Born approximation and Green's function for the wave equation, the analytical inverse scattering problem can be defined in matrix-vector form. Adopting this setting, it has been suggested in the past to reduce the correlation between the samples of the measurement using Cylindrical Waves (CWs) with randomly selected delays and weights. In a similar setting, we created an optimization problem accepting transmission delays and weights as variables to minimize the correlation between the samples of the measurement in each receiver. We demonstrate via simulations that CWs employing the optimized transmission parameters outperformed the cases with Plane Wave Imaging (PWI) and CWs with random transmission parameters in terms of reconstruction accuracy.**

***Index Terms*—inverse scattering problem, optimized incident waves, sparse signal recovery, fast pulse-echo ultrasound imaging**

I. Introduction

Ultrasound signals are being employed in areas like medical imaging [1], non-destructive testing (NDT) [2], communication [3] and navigation [4]. In many of these application areas, it is required to have real-time systems. Therefore, fast data acquisition without sacrificing the accuracy of the signal reconstruction is crucial.

There are several recent approaches attempting to overcome the trade-off between reconstructed ultrasound image quality and data acquisition speed by accepting single pulse-echo measurement. These approaches mostly perform deep learning techniques [5] and sparse signal recovery [6], [7] methods. Although the sparse signal recovery methods achieve good reconstruction accuracy, this can still be improved by reducing the correlation between the different samples of the pulse-echo measurements.

This work was partially supported by the Fraunhofer Internal Programs under Grant No. Attract 025-601128, the German Research Council (DFG) under the project "CoSMaDu", as well as the Thuringian Ministry of Economic Affairs, Science and Digital Society (TMWWDG).

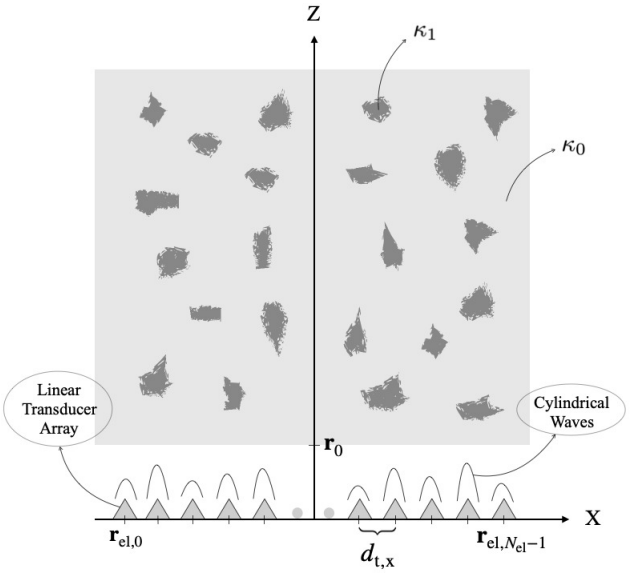

Fig. 1. 2D inhomogeneous reconstruction area with partial cracks holding the compressibility value κ_1 inside the covering material with compressibility κ_0.

In ultrasound imaging, the system of linear equations addressed in sparse signal recovery methods exploiting the sparsity of material properties of measurement area can be derived via the Lippmann-Schwinger equation [8] meeting the Sommerfeld radiation condition [9]. The feasibility and the estimation accuracy of the sparse signal recovery algorithms depend on the sparsity level of the estimated signals defined in an appropriate domain and the correlation between the different samples of the pulse-echo measurements received by the individual receivers. In the related works [6], [7], pulse-echo ultrasound imaging based on sparse recovery adopting Plane Wave Imaging (PWI) in the Fourier domain was introduced without any attempt to decrease the correlation between the samples of the single pulse-echo measurement. In [10], [11], this correlation was reduced by transmitting randomly weighted and delayed Cylindrical Waves (CWs). In our paper, an optimization algorithm forcing the transmitters to minimize the correlation between different pulse-echo samples in the Fourier domain by choosing optimum delays and weights for transmitted CWs is introduced.

In the following sections, a physical model of the sparse

inhomogeneities of the reconstruction area is defined. Then, a model for inverse scattering and sparse signal recovery problems is described. Afterward, the optimization process of the transmitted CWs, which is the contribution of the work, is formulated. Lastly, the simulation parameters are specified, and the performance results of the proposed method based on the simulation model are demonstrated.

II. Physical Model

In this part, the pulse-echo signal is written as a function of the transmission parameters in order to design an optimization problem afterward minimizing the correlation between different samples of the pulse-echo measurements.

A. Model of the Reconstruction Area

The reconstruction of the material parameters inside a certain reconstruction area is aimed to realize via the waves passed through the corresponding volume. The reconstruction area as seen in Fig. 1 is assumed to be homogeneous with compressibility κ_0 outside inhomogeneous regions which scatter the incident waves without dispersion and absorption in accordance with the first order Born approximation [12], and have constant compressibility κ_1. Those inhomogeneous regions have the coordinates defined by the set $\zeta \subset \{(\mathrm{x},\mathrm{z}) : \mathrm{x} \in \mathbb{R},\ \mathrm{z} \in \mathbb{R}^+\}$. The relative spatial fluctuations in the reconstruction area can be defined as

$$\gamma(\mathbf{r}) = \begin{cases} 1-\kappa_1(\mathbf{r})/\kappa_0 & \text{for } \mathbf{r} \in \zeta, \\ 0 & \text{for } \mathbf{r} \notin \zeta, \end{cases} \tag{1}$$

while $\mathbf{r} \in \mathbb{R}^2$. The assumption of the sparsity of $\gamma(\mathbf{r})$ enables sparse recovery.

The reconstruction area in the implementation is discretized using standard unit vectors $\mathbf{e}_\mathrm{x}$ and $\mathbf{e}_\mathrm{z}$ as

$$\begin{aligned}\mathcal{Z} = \{\mathbf{r}_i \in \mathbb{R}^2 \setminus \{\mathrm{z} \le 0\} : \mathbf{r}_i = \mathbf{r}_0 + i_\mathrm{x} d_\mathrm{x}\mathbf{e}_\mathrm{x} + i_\mathrm{z} d_\mathrm{z}\mathbf{e}_\mathrm{z}, \\ 0 \le i_\mathrm{x} < N_\mathrm{x}, 0 \le i_\mathrm{z} < N_\mathrm{z}, i = i_\mathrm{z}N_\mathrm{x} + i_\mathrm{x}\}\end{aligned} \tag{2}$$

where $\mathbf{r}_0$ is the offset vector, $d_\mathrm{x}, d_\mathrm{z}$ are the distances between two grid points and $N_\mathrm{x}, N_\mathrm{z}$ are the number of grid points on x and z-axis correspondingly. Lastly, the set of transducer coordinates of the uniform linear array (ULA) can be defined as

$$\begin{aligned}\mathcal{M} = \{\mathbf{r}_{\mathrm{el},m} \in \mathbb{R}^2 : \mathbf{r}_{\mathrm{el},m} = (m - 0.5(N_\mathrm{el}-1)d_\mathrm{t,x})\,\mathbf{e}_\mathrm{x}, \\ 0 \le m < N_\mathrm{el}\}\end{aligned} \tag{3}$$

where $d_\mathrm{t,x}$ is the element distance, and N_el is the number of transducer elements.

B. Formulation of Inverse Scattering Problem

Exploiting the affect of time delay on the Fourier domain $u_m(n-\tau_m) \xrightarrow{\mathcal{F}} u_m(\ell)e^{-j\omega_\ell\tau_m}$, the incident acoustic pressure in each transmitter m employing the pulse with discrete angular frequency ω_ℓ in the Fourier basis can be formulated as

$$p_{m,\ell} = a_m u_{m,\ell} e^{-j\omega_\ell\tau_m} \tag{4}$$

where $0 \le \ell < N_\mathrm{f}$ is the discrete frequency index, $a_m \in \mathbb{R}$ is the transmission weight, $u_{m,\ell} \triangleq u_m(\ell)$ is the ℓ-th Fourier coefficient of the transmitted pulse, τ_m is the time delay of the m-th transmitter and N_f is the number of frequency indices. Then, the incident acoustic pressure field which is a result of all transmitters transmitting at the same time, each with their own delay and weight can be derived as

$$p_\ell^\mathrm{in}(\mathbf{r}_i) = \sum_{m=0}^{N_\mathrm{el}-1} p_{m,\ell}\; g_\ell(\mathbf{r}_i - \mathbf{r}_{\mathrm{el},m}) \tag{5}$$

with the help of the free-space Green's function $g_\ell(\mathbf{r}) = \frac{j}{4}H_0^{(2)}(k_\ell\|\mathbf{r}\|_2)$ [13, (2.14) and (2.19)] derived from the solution of inhomogeneous Helmholtz equations $(\Delta + k_\ell^2)g_\ell(\mathbf{r}) = \delta(\mathbf{r})$ [14, (47)] satisfying Sommerfeld radiation conditions, where $H_0^{(2)}$ is the zero order Hankel function of second kind [15, (§10.2(ii)) and (10.4.3)], $k_\ell = \omega_\ell/c_0$, c_0 is the sound speed in the homogenous medium, $\|\mathbf{r}\|_2$ represents the ℓ_2 norm of $\mathbf{r}$, and $\delta(\mathbf{r})$ denotes a two-dimensional unit impulse.

After modeling the incident acoustic pressure, the scattered acoustic pressure for a single discrete frequency can be determined with the help of the Born approximation [12] as

$$p_\ell^\mathrm{sc}(\mathbf{r}) \approx k_\ell^2 \int_\zeta \gamma(\mathbf{r}')p_\ell^\mathrm{in}(\mathbf{r}')g_\ell(\mathbf{r}-\mathbf{r}')d\mathbf{r}', \tag{6}$$

which can be discretized with (2) and (3), and turned into

$$p_\ell^\mathrm{sc}(\mathbf{r}_{\mathrm{el},m}) = k_\ell^2\Delta A' \sum_{i=0}^{N_\mathrm{grid}-1} \gamma(\mathbf{r}_i)p_\ell^\mathrm{in}(\mathbf{r}_i)g_\ell(\mathbf{r}_{\mathrm{el},m}-\mathbf{r}_i) \tag{7}$$

where $\Delta A' = d_\mathrm{x}d_\mathrm{z}$ and $N_\mathrm{grid} = N_\mathrm{x}N_\mathrm{z}$.

C. Design of Sparse Signal Recovery Problem

In this section, the definition of the model matrix as $\mathbf{G}_\ell(\mathbf{a},\boldsymbol{\tau}) \triangleq \mathbf{G}_{R_\ell}\,\mathrm{Diag}(\mathbf{G}_{T_\ell}\mathbf{p}_\ell) = \mathbf{G}_{R_\ell}\,\mathrm{Diag}(\mathbf{G}_{T_\ell}(\mathbf{u}_\ell \odot \mathbf{a} \odot e^{-j\omega_\ell\boldsymbol{\tau}}))$ is introduced where $\mathbf{G}_{T_\ell} \in \mathbb{C}^{N_\mathrm{grid}\times N_\mathrm{el}}$ contains $g_\ell(\mathbf{r}_i - \mathbf{r}_{\mathrm{el},m})$ on i-th row and m-th column, $\mathbf{G}_{R_\ell} \triangleq k_\ell^2\Delta A'\mathbf{G}_{T_\ell}^T$, $\mathbf{p}_\ell$, $\mathbf{u}_\ell$, $\mathbf{a}$, $\boldsymbol{\tau} \in \mathbb{C}^{N_\mathrm{el}\times 1}$ are the column vectors containing $p_{m,\ell}$, $u_{m,\ell}$, a_m and τ_m in each row m correspondingly, $\odot$ denotes element-wise multiplication and $\mathrm{Diag}(\cdot)$ operator constructs a diagonal matrix from the argument vector. For convenience, $\mathbf{G}_\ell$ will be used instead of $\mathbf{G}_\ell(\mathbf{a},\boldsymbol{\tau})$ in the following part. Then, the pulse-echo signals at the receiver elements in (7) can be denoted in matrix-vector form as

$$\mathbf{p}^\mathrm{sc} = \begin{pmatrix} \mathbf{G}_0 \\ \vdots \\ \mathbf{G}_{N_\mathrm{f}-1} \end{pmatrix}\boldsymbol{\gamma} + \boldsymbol{\eta} = \mathbf{G}\boldsymbol{\gamma} + \boldsymbol{\eta}, \tag{8}$$

with the addition of $\boldsymbol{\eta} \in \mathbb{C}^{N_\mathrm{el}N_\mathrm{f}\times 1}$, which is the result of random perturbations like measurement noise, and $\boldsymbol{\gamma} \in \mathbb{R}^{N_\mathrm{grid}\times 1}$ is the vector containing the relative fluctuations $\gamma(\mathbf{r})$ in each element. Modeling the single pulse-echo measurement data with (8), the target is to estimate $\boldsymbol{\gamma}$ given $\boldsymbol{p}^\mathrm{sc}$ by exploiting the sparsity of $\boldsymbol{\gamma}$. This can be realized via the basis pursuit denoising problem [16] for which the problem is formulated as

$$\hat{\boldsymbol{\gamma}} = \underset{\boldsymbol{\gamma}\in\mathbb{C}^{N_\mathrm{el}\times 1}}{\arg\min}\ \|\boldsymbol{\gamma}\|_1 \quad \text{s. t.} \quad \|\mathbf{p}^\mathrm{sc} - \mathbf{G}\boldsymbol{\gamma}\|_2 \le \eta, \tag{9}$$

where $\|\boldsymbol{\eta}\|_2 \le \eta$.

III. Derivation of Optimized Transmission Parameters

One of the factors affecting the estimation accuracy of the sparsity-promoting algorithms is the correlation between the samples of the single pulse-echo measurement at each receiver. Since the constructed model has predefined material properties and signal bandwidth, only weights and delays of the transmitted signal can be controlled in our model to minimize the correlation between the received samples. The maximum amount of the time delay should also be kept considerably smaller than the total recording time by regarding the additional time-of-flight. Then, the constrained optimization problem minimizing this correlation together with limiting the range of optimized delay vector $\mathbf{0} \leq \boldsymbol{\tau}_{\text{opt}} \leq \mathbf{1}\tau_{\max}$ by utilizing the logarithmic barrier function can be defined as

$$\begin{aligned}\mathbf{a}_{\text{opt}}, \boldsymbol{\tau}_{\text{opt}} &= \underset{\mathbf{a},\boldsymbol{\tau}}{\operatorname{argmin}} \big(\|\mathbf{G}^H(\mathbf{a},\boldsymbol{\tau})\mathbf{G}(\mathbf{a},\boldsymbol{\tau}) - \mathbf{I}_{N_{\text{grid}}}\|_{\text{F}}^2 \\ &\quad -\mathbf{1}^T \left(\log\left(\mathbf{1}\tau_{\max} - \boldsymbol{\tau}\right) + \log(\boldsymbol{\tau})\right)\big) \\ &= \underset{\mathbf{a},\boldsymbol{\tau}}{\operatorname{argmin}} \left(A(\mathbf{a},\boldsymbol{\tau}) + B(\boldsymbol{\tau})\right)\end{aligned} \tag{10}$$

where the vectors $\mathbf{0},\ \mathbf{1} \in \mathbb{R}^{N_{\text{el}}\times 1}$ includes 0 and 1 in each element correspondingly, the identity matrix $\mathbf{I}_{N_{\text{grid}}} \in \mathbb{R}^{N_{\text{grid}}\times N_{\text{grid}}}$ is selected as target value of the objective function among other choices of orthogonal matrices as in [17] for the sake of simplicity of gradient calculations, and $A(\mathbf{a},\boldsymbol{\tau})$, $B(\boldsymbol{\tau})$ represent the first and second part of the objective function. Afterwards, the first part of the objective function without the logarithmic barrier function is reformulated as

$$\begin{aligned}A &= \left\|\mathbf{G}^H\mathbf{G} - \mathbf{I}_{N_{\text{grid}}}\right\|_{\text{F}}^2 \\ &= \operatorname{Tr}\left(\left(\mathbf{G}^H\mathbf{G} - \mathbf{I}_{N_{\text{grid}}}\right)\left(\mathbf{G}^H\mathbf{G} - \mathbf{I}_{N_{\text{grid}}}\right)\right) \\ &= \operatorname{Tr}\left(\left(\mathbf{G}^H\mathbf{G} - \mathbf{I}\right)\left(\mathbf{G}^H\mathbf{G} - \mathbf{I}\right)\right) \\ &= \operatorname{Tr}\Big(\sum_{\ell=0}^{N_{\text{f}}-1}\left(\mathbf{G}_\ell^H\mathbf{G}_\ell - \mathbf{I}/N_{\text{f}}\right)\sum_{k=0}^{N_{\text{f}}-1}\left(\mathbf{G}_k^H\mathbf{G}_k - \mathbf{I}/N_{\text{f}}\right)\Big) \\ &= \operatorname{Tr}\Big(\sum_{\ell=0}^{N_{\text{f}}-1}\left(\mathbf{G}_\ell^H\mathbf{G}_\ell\right)\left(\mathbf{G}_\ell^H\mathbf{G}_\ell\right)\Big) \\ &\quad + \operatorname{Tr}\Big(\sum_{\ell=0}^{N_{\text{f}}-1}\sum_{k=0,k\neq\ell}^{N_{\text{f}}-1}\left(\mathbf{G}_\ell^H\mathbf{G}_\ell\right)\left(\mathbf{G}_k^H\mathbf{G}_k\right)\Big) \\ &\quad - \operatorname{Tr}\Big(2\sum_{\ell=0}^{N_{\text{f}}-1}\left(\mathbf{G}_\ell^H\mathbf{G}_\ell\right)\Big) + \Big(N_{\text{grid}}\Big) \\ &= f_1 + f_2 + f_3 + f_4\end{aligned} \tag{11}$$

where k represents the discrete frequency index and $\mathbf{I}_{N_{\text{grid}}}$ was called as $\mathbf{I}$ for convenience. Additionally, the equalities $\|\boldsymbol{X}\|_{\text{F}}^2 = \operatorname{Tr}(\boldsymbol{X}^H\boldsymbol{X})$ and $\operatorname{Tr}(\mathbf{X}+\mathbf{Y}) = \operatorname{Tr}(\mathbf{X}) + \operatorname{Tr}(\mathbf{Y})$ are exploited in (11) while $\mathbf{X}$ and $\mathbf{Y}$ are suitably shaped matrices.

Since the gradient descent [18] algorithm is employed in the optimization, the gradients of the objective function with respect to transmission weights and time delays should be formulated. Employing the chain rule of Wirtinger derivatives [19], the gradient of the A with respect to the weights is divided into parts with different gradient formulas and formulated as

$$\begin{aligned}\frac{\partial A}{\partial \mathbf{a}} &= \frac{\partial f_1}{\partial \mathbf{a}} + \frac{\partial f_2}{\partial \mathbf{a}} + \frac{\partial f_3}{\partial \mathbf{a}} + \frac{\partial f_4}{\partial \mathbf{a}} \\ &= \sum_{m=1}^{4}\sum_{\ell=0}^{N_{\text{f}}-1}\left(\left(\frac{\partial f_m}{\partial \mathbf{b}_\ell}\right)^T\frac{\partial \mathbf{b}_\ell}{\partial \mathbf{a}} + \left(\frac{\partial f_m}{\partial \mathbf{b}_\ell^*}\right)^T\frac{\partial \mathbf{b}_\ell^*}{\partial \mathbf{a}}\right)^T \\ &= 2\sum_{m=1}^{4}\sum_{\ell=0}^{N_{\text{f}}-1}\operatorname{Re}\left(\left(\frac{\partial f_m}{\partial \mathbf{b}_\ell}\right)^T\frac{\partial \mathbf{b}_\ell}{\partial \mathbf{a}}\right)^T,\end{aligned} \tag{12}$$

and the gradient with respect to time delays considering the gradient of the logarithmic barrier function turns out to

$$\begin{aligned}\frac{\partial A}{\partial \boldsymbol{\tau}} + \frac{\partial B}{\partial \boldsymbol{\tau}} &= 2\sum_{m=1}^{4}\sum_{\ell=0}^{N_{\text{f}}-1}\operatorname{Re}\left(\left(\frac{\partial f_m}{\partial \mathbf{b}_\ell}\right)^T\frac{\partial \mathbf{b}_\ell}{\partial \boldsymbol{\tau}}\right)^T \\ &\quad + \left(\mathbf{1} \oslash \left(\mathbf{1}\tau_{\max} - \boldsymbol{\tau}\right)\right) - \left(\mathbf{1} \oslash \boldsymbol{\tau}\right),\end{aligned} \tag{13}$$

where $(\cdot)^*$ is complex conjugate, $\oslash$ denotes element-wise division, $\mathbf{b}_\ell = \mathbf{G}_{T_\ell}\mathbf{p}_\ell$, $\frac{\partial f_m}{\partial \mathbf{b}_\ell} \in \mathbb{C}^{N_{\text{grid}}\times 1}$ and the Jacobian matrices of $\mathbf{b}_\ell$ are $\frac{\partial \mathbf{b}_\ell}{\partial \mathbf{a}}$, $\frac{\partial \mathbf{b}_\ell}{\partial \boldsymbol{\tau}} \in \mathbb{C}^{N_{\text{grid}}\times N_{\text{el}}}$.

The gradients $\partial f_m/\partial \mathbf{b}_\ell$ for each index m are presented in the following part. Firstly, f_1 is rewritten as

$$\begin{aligned}f_1 = \sum_{\ell=0}^{N_{\text{f}}-1}&\operatorname{Tr}\left(\operatorname{Diag}\left(\mathbf{b}_\ell^*\right)\mathbf{G}_{R_\ell}^H\mathbf{G}_{R_\ell}\operatorname{Diag}\left(\mathbf{b}_\ell \odot \mathbf{b}_\ell^*\right)\right. \\ &\left.\mathbf{G}_{R_\ell}^H\mathbf{G}_{R_\ell}\operatorname{Diag}\left(\mathbf{b}_\ell\right)\right),\end{aligned} \tag{14}$$

with which $\partial f_1/\partial \mathbf{b}_\ell$ is found to be

$$\begin{aligned}\frac{\partial f_1}{\partial \mathbf{b}_\ell} &= 2\operatorname{diag}\left(\mathbf{G}_{R_\ell}^H\mathbf{G}_{R_\ell}\operatorname{Diag}\left(\mathbf{b}_\ell \odot \mathbf{b}_\ell^*\right)\right. \\ &\quad \left.\mathbf{G}_{R_\ell}^H\mathbf{G}_{R_\ell}\right) \odot \mathbf{b}_\ell^*,\end{aligned} \tag{15}$$

where $\operatorname{diag}(\cdot)$ operator constructs a vector from the diagonal elements of the argument matrix. Expanding the f_2 as

$$\begin{aligned}f_2 = \sum_{\ell=0}^{N_{\text{f}}-1}\sum_{k=0,k\neq\ell}^{N_{\text{f}}-1}&\operatorname{Tr}\left(\operatorname{Diag}\left(\mathbf{b}_\ell^*\right)\mathbf{G}_{R_\ell}^H\mathbf{G}_{R_\ell}\right. \\ &\left.\operatorname{Diag}\left(\mathbf{b}_\ell \odot \mathbf{b}_k^*\right)\mathbf{G}_{R_k}^H\mathbf{G}_{R_k}\operatorname{Diag}\left(\mathbf{b}_k\right)\right),\end{aligned} \tag{16}$$

the gradient $\partial f_2/\partial \mathbf{b}_\ell$ can be determined as

$$\begin{aligned}\frac{\partial f_2}{\partial \mathbf{b}_\ell} &= \sum_{k=0,k\neq\ell}^{N_{\text{f}}-1} 2\left(\operatorname{diag}\left(\mathbf{G}_{R_\ell}^H\mathbf{G}_{R_\ell}\operatorname{Diag}\left(\mathbf{b}_\ell^* \odot \mathbf{b}_k\right)\right.\right. \\ &\quad \left.\left.\mathbf{G}_{R_k}^H\mathbf{G}_{R_k}\right) \odot \mathbf{b}_k^*\right).\end{aligned} \tag{17}$$

The third summand f_3 and its gradient $\frac{\partial f_3}{\partial \mathbf{b}_\ell}$ is derived as

$$f_3 = -2\operatorname{Tr}\Big(\sum_{\ell=0}^{N_{\text{f}}-1}\operatorname{Diag}\left(\mathbf{b}_\ell^*\right)\mathbf{G}_{R_\ell}^H\mathbf{G}_{R_\ell}\operatorname{Diag}\left(\mathbf{b}_\ell\right)\Big) \tag{18}$$

$$\frac{\partial f_3}{\partial \mathbf{b}_\ell} = -2\left(\operatorname{diag}\left(\mathbf{G}_{R_\ell}^H\mathbf{G}_{R_\ell}\right) \odot \mathbf{b}_\ell^*\right). \tag{19}$$

Since the last part of the objective function f_4 is constant, its gradient

$$\frac{\partial f_4}{\partial \mathbf{b}_\ell} = \mathbf{0}. \tag{20}$$

Lastly, the Jacobian matrix of the $\mathbf{b}_\ell$ with respect to the transmission weight vector $\mathbf{a}$ and time delay vector $\boldsymbol{\tau}$ can be determined as

$$\frac{\partial \mathbf{b}_\ell}{\partial \mathbf{a}} = \mathbf{G}_{T_\ell} \ \mathrm{Diag}\left(\mathbf{u}_\ell \odot e^{-j\omega_\ell \boldsymbol{\tau}}\right), \tag{21}$$

$$\frac{\partial \mathbf{b}_\ell}{\partial \boldsymbol{\tau}} = \mathbf{G}_{T_\ell} \ \mathrm{Diag}\left(\mathbf{a} \odot \mathbf{u}_\ell \odot \left(-j\omega_\ell e^{-j\omega_\ell \boldsymbol{\tau}}\right)\right). \tag{22}$$

Having defined all the necessary quantities, the optimization problem (10) is tackled via gradient descent algorithm [18]

$$\mathbf{a}_{n+1} = \mathbf{a}_n - \chi_n^{\mathrm{a}} \frac{\partial}{\partial \mathbf{a}_n} A(\mathbf{a}_n, \boldsymbol{\tau}_n), \tag{23}$$

$$\boldsymbol{\tau}_{n+1} = \boldsymbol{\tau}_n - \chi_n^{\tau} \frac{\partial}{\partial \boldsymbol{\tau}_n} \left(A(\mathbf{a}_n, \boldsymbol{\tau}_n) + B(\boldsymbol{\tau}_n)\right), \tag{24}$$

where χ_n^{a} and χ_n^{τ} are the adaptive step sizes in iteration n.

IV. Performance Evaluation

A. Simulation Parameters

The imaging area is chosen as the two-dimensional xz-plane where the x-axis is selected for the transducer elements, and xz-plane is selected for the measurement area as defined in (2) and (3). The offset vector $\mathbf{r}_0 = 15 \times 10^{-3} \mathbf{e}_z$ in meters, the distances between the transducer elements $d_{\mathrm{t,x}} = 625\,\mu\mathrm{m}$, and the distances between the grid points inside the measurement area d_{x} and d_{z} are chosen as $312.5\,\mu\mathrm{m}$. The number of transducer elements $N_{\mathrm{el}} = 16$, and the numbers of grid points in the x and z directions of the measurement area are $N_x = N_z = 32$. The reference speed of sound $c_0 = 1500$ m/s, the relative spatial fluctuations $\gamma(\mathbf{r}) = 0.1$ while $\mathbf{r} \notin \zeta$, and ζ is composed of an equidistant 2-D grid of $6 \times 6 = 36$ scattering locations at the indices $(m_x, m_z) \in [7, 17, ..., 57]^2$, cf. Figure 3, inspired by the setup in [10]. We consider a sinc-shaped pulse, which is modulated to a center frequency of $f_{\mathrm{c}} = 5\,\mathrm{MHz}$, and $N_{\mathrm{f}} = 80$ discrete frequencies from its bandwidth are exploited. We choose a total recording time of $T_{\mathrm{rec}} = 80\,\mu\mathrm{s}$ which corresponds to a frequency resolution of $f_0 = 1/T_{\mathrm{rec}} = 12.5\,\mathrm{kHz}$ in our simulation. Then, the set of discrete frequencies $f_\ell = w_\ell/(2\pi)$ is defined as

$$\xi = \{f_\ell \in \ \mathbb{R}^+ : \ f_\ell = f_{\mathrm{c}} + f_0(\ell - 0.5N_{\mathrm{f}}), \\ 0 \leq \ell < N_{\mathrm{f}}\}. \tag{25}$$

The discrete Fourier coefficients of the pulse are $u_{m,\ell} = 1$ for $0 \leq \ell < N_{\mathrm{f}}$ since the frequency response of the sinc pulse gives a constant value.

Afterward, the simulated medium is insonified with different transmission schemes, with the goal to estimate the sparse spatial fluctuations. This task is formulated as in (9) and tackled with fast iterative shrinkage-thresholding algorithm (FISTA) [20] running 36 iterations which are equal to the cardinality of the set ζ. The random perturbations $\boldsymbol{\eta}$ on the receivers is multivariate complex Gaussian noise with the distribution $\mathcal{CN}(\mathbf{0}, c\mathbf{I})$ while $c = 10^{-2}$.

The gradient descent algorithm in (23) and (24) is randomly initialized such that the delays are uniformly distributed in the range $0 \leq \tau_m < \tau_{\max}$ where $\tau_{\max} = 20\,\mu\mathrm{s}$ and $a_m \sim \mathcal{N}(0, 1)$.

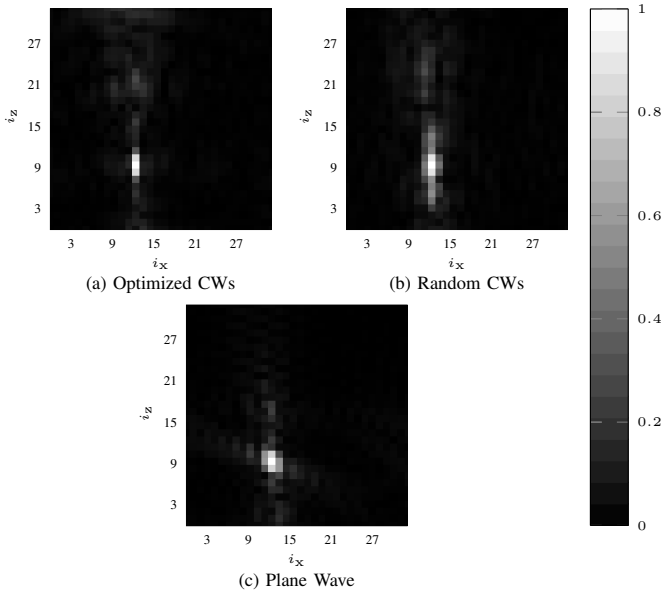

Fig. 2. Mutual correlation coefficient map of the column vectors of the $\mathbf{G}$ matrix with a representative j-th column vector where arbitrary indices $j_x = 12$ and $j_z = 9$ for three different scenarios (a) optimized CWs, (b) random CWs and (c) plane wave.

The adaptive step sizes χ_n^{a} and χ_n^{τ} are updated in each iteration n of the gradient descent by applying the Armijo rule [21].

Lastly, the results of the CWs with optimized transmission delays and weights are compared with the results obtained for PWI and randomly delayed and weighted CWs as similar to approaches in [10]. In the case of PWI, the amplitude of the m-th transmitter element $a_m = 1$ and the time delay for each transmitter m is distributed as $\tau_{\max} - (N_{el} d_{t,x} sin(\theta)/c_0) + m d_{t,x} sin(\theta)/c_0$ while the angle between planar wavefront and e_{x} is $\theta = \pi/3$. For the randomly delayed and weighted CWs, transmission delays and weights in each transducer are assigned as $0 \leq \tau_m < \tau_{\max}$ while τ_m is uniformly distributed, and $a_m \sim \mathcal{N}(0, 1)$. In both PWI and randomly delayed and weighted CWs, the transmission weight vector is scaled as $\mathbf{a} = (\mathbf{a}/\|\mathbf{a}\|_2)\|\mathbf{a}_{\mathrm{opt}}\|_2$ to make the transmit power equal for three scenarios.

B. Simulation Results

In this section, the performance of the CWs with optimized delays and weights is validated by comparing them against PWI and the CWs with random delays and weights.

The first results quantify the coherence of the matrix $\mathbf{G}$ by calculating the mutual correlation coefficient of its columns as

$$c(i, j) = \frac{\mathbf{g}_i^H \mathbf{g}_j}{\|\mathbf{g}_i\|_2 \|\mathbf{g}_j\|_2}, \tag{26}$$

where i, j are the indices of the reconstruction area in (2) and the arbitrary constant $j = j_{\mathrm{z}} N_{\mathrm{x}} + j_{\mathrm{x}} = 300$ is chosen to represent the mutual correlation coefficient where $j_{\mathrm{z}} = 9$ and $j_{\mathrm{x}} = 12$. As shown in Fig. 2, the CWs with optimized delays and amplitudes have lower mutual correlations compared to pseudo-random CWs and PWI scenarios which shows that the

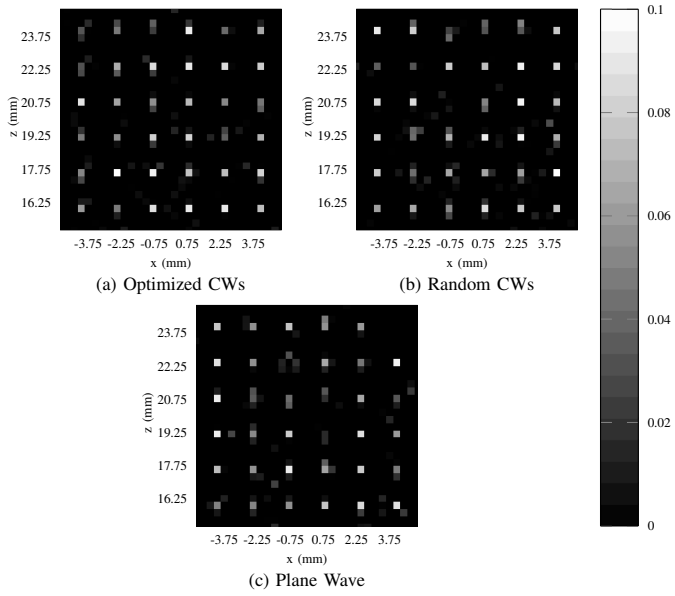

(a) Optimized CWs (b) Random CWs

(c) Plane Wave

Fig. 3. Reconstruction result comparison of the three different cases where (a) optimized CWs, (b) random CWs and (c) plane wave.

optimization algorithm defined in (10) enables the reduction of the coherence.

The subsequent result is related to the reconstruction accuracy of the spatial fluctuations obtained by the three different approaches of choosing the transmitted signal parameters. It can be noticed in Fig. 3 that the suggested method outperforms the other cases in terms of reconstruction accuracy in the conditions of the simulation model. However, the proposed optimization method still have difficulty to estimate the locations of some points which can be related to the non-convex cost function of the optimization problem defined in (10), since the performance of the non-convex optimization is affected by the initialization of the gradient-based algorithms. Another reason for missing the exact scatterer locations is the additive random perturbations in (8) which affect the FISTA algorithm estimation performance.

V. Conclusion

In this paper, transmission delays and weights are optimized in the Fourier domain to minimize the correlation between distinct received signals when using ULAs for multi-channel ultrasound imaging. Through explicit analytical expressions of the gradients, an iterative gradient-based algorithm can be applied to find the optimal parameters. The simulation results demonstrate a reduction in the mutual correlations compared to plane-wave imaging and a pseudo-random choice of delays and weights. Additionally, the proposed method demonstrates a better estimation accuracy in terms of scatterer localization compared to the state-of-the-art, which indicates that the sparsity-promoting algorithm benefits from a reduced correlation between the received signals. The method can also easily be adapted to multiple sequential pulse-echo measurements. Besides, it requires no prior knowledge of the compressibility values of the materials, and thus multiple signal reconstructions can be achieved once the optimized parameters are obtained. As further work, the optimization problem may be validated with experimental data gathered from NDT applications following the adaption to more comprehensive mathematical models without the omission of spatial amplitude absorption and the assumption of pure homogenous measurement medium outside the defects.

References

[1] J. W. Hunt, M. Arditi, and F. S. Foster, "Ultrasound transducers for pulse-echo medical imaging," *IEEE Transactions on Biomedical Engineering*, no. 8, pp. 453–481, 1983.

[2] L. Le Jeune, S. Robert, E. L. Villaverde, and C. Prada, "Plane wave imaging for ultrasonic non-destructive testing: Generalization to multi-modal imaging," *Ultrasonics*, vol. 64, pp. 128–138, 2016.

[3] S. Holm, O. B. Hovind, S. Rostad, and R. Holm, "Indoors data communications using airborne ultrasound," in *Proceedings.(ICASSP'05). IEEE International Conference on Acoustics, Speech, and Signal Processing, 2005.*, vol. 3. IEEE, 2005, pp. iii–957.

[4] Q. Wang, K. F. Chan, K. Schweizer, X. Du, D. Jin, S. C. H. Yu, B. J. Nelson, and L. Zhang, "Ultrasound doppler-guided real-time navigation of a magnetic microswarm for active endovascular delivery," *Science Advances*, vol. 7, no. 9, p. eabe5914, 2021.

[5] G. Pilikos, C. L. de Korte, T. van Leeuwen, and F. Lucka, "Single plane-wave imaging using physics-based deep learning," in *2021 IEEE International Ultrasonics Symposium (IUS)*. IEEE, 2021, pp. 1–4.

[6] M. F. Schiffner and G. Schmitz, "Fast pulse-echo ultrasound imaging employing compressive sensing," in *2011 IEEE International Ultrasonics Symposium*. IEEE, 2011, pp. 688–691.

[7] M. F. Schiffner and G. Schmitz, "Pulse-echo ultrasound imaging combining compressed sensing and the fast multipole method," in *2014 IEEE International Ultrasonics Symposium*. IEEE, 2014, pp. 2205–2208.

[8] B. A. Lippmann and J. Schwinger, "Variational principles for scattering processes. i," *Physical Review*, vol. 79, no. 3, p. 469, 1950.

[9] A. Sommerfeld, *Partial differential equations in physics*. Academic press, 1949.

[10] M. F. Schiffner and G. Schmitz, "Fast compressive pulse-echo ultrasound imaging using random incident sound fields," *The Journal of the Acoustical Society of America*, vol. 141, no. 5, pp. 3611–3611, 2017.

[11] M. F. Schiffner, "Random incident waves for fast compressed pulse-echo ultrasound imaging," *arXiv preprint arXiv:1801.00205*, 2017.

[12] J. Gubernatis, E. Domany, J. Krumhansl, and M. Huberman, "The born approximation in the theory of the scattering of elastic waves by flaws," *Journal of Applied Physics*, vol. 48, no. 7, pp. 2812–2819, 1977.

[13] A. J. Devaney, *Mathematical foundations of imaging, tomography and wavefield inversion*. Cambridge University Press, 2012.

[14] F. Natterer and F. Wübbeling, *Mathematical Methods in Image Reconstruction*. SIAM, 2001.

[15] F. W. Olver, D. W. Lozier, R. F. Boisvert, and C. W. Clark, *NIST handbook of mathematical functions hardback and CD-ROM*. Cambridge University Press, 2010.

[16] S. Chen and D. Donoho, "Basis pursuit," in *Proceedings of 1994 28th Asilomar Conference on Signals, Systems and Computers*, vol. 1. IEEE, 1994, pp. 41–44.

[17] J. M. Duarte-Carvajalino and G. Sapiro, "Learning to sense sparse signals: Simultaneous sensing matrix and sparsifying dictionary optimization," *IEEE Transactions on Image Processing*, vol. 18, no. 7, pp. 1395–1408, 2009.

[18] H. B. Curry, "The method of steepest descent for non-linear minimization problems," *Quarterly of Applied Mathematics*, vol. 2, no. 3, pp. 258–261, 1944.

[19] W. Wirtinger, "Zur formalen theorie der funktionen von mehr komplexen veränderlichen," *Mathematische Annalen*, vol. 97, no. 1, pp. 357–375, 1927.

[20] A. Beck and M. Teboulle, "A fast iterative shrinkage-thresholding algorithm for linear inverse problems," *SIAM journal on imaging sciences*, vol. 2, no. 1, pp. 183–202, 2009.

[21] L. Armijo, "Minimization of functions having lipschitz continuous first partial derivatives," *Pacific Journal of Mathematics*, vol. 16, no. 1, pp. 1–3, 1966.